

Optical absorption in quantum dots: Coupling to longitudinal optical phonons treated exactly

T. Stauber¹ and R. Zimmermann²

¹*Instituto de Ciencia de Materiales de Madrid, CSIC, Cantoblanco, E-28049 Madrid, Spain*

²*Institut für Physik, Humboldt-Universität zu Berlin, Newtonstrasse 15, D-12489 Berlin, Germany*

(Dated: February 8, 2020)

Optical transitions in a semiconductor quantum dot are theoretically investigated, with emphasis on the coupling to longitudinal optical phonons. When limiting to a finite number m of electron and hole levels in the dot, the model can be solved exactly within numerical accuracy. Crucial for this to work is the absence of dispersion of the phonons, which allows a transformation leaving only $m(m+1) - 2$ phonon modes to be coupled to the electronic system. We calculate the linear optical polarization following a delta pulse excitation, and by a subsequent Fourier transformation the resulting optical absorption. This strict result is compared with a frequently used approximation modelling the absorption as a convolution between spectral functions of electron and hole, which tends to overestimate the effect of the phonon coupling. Numerical results are given for two electron and hole states in a quantum dot made from the polar material CdSe. Parameter values are chosen such that a quantum dot with a resonant sublevel distance can be compared with a nonresonant one.

I. INTRODUCTION

Quantum dots (QDs) based on semiconductor structures have received great attention for almost two decades now [1]. Whereas early experiments were only able to measure ensemble averages over many quantum dots, it is nowadays possible to address single quantum dots individually [2]. While earlier measurements were concentrating on photoluminescence, recently absorption spectra have been measured [3] with high spatial resolution showing distinct lines related to individual dots (due to well width fluctuations). Using photoluminescence spectroscopy and magnetic fields, detailed information on energy levels and phonon coupling could be extracted for single QDs made from II-IV semiconductor material [4]. This and related experimental work has enormously stimulated investigations on the interaction between the carriers on confinement levels and the surrounding polarizable medium on a microscopic level. A proper understanding of the related dephasing mechanisms might become important in view of future quantum computation applications based on semiconductor quantum dots.

Carrier relaxation and dephasing in quantum dots crucially depends on the interaction with lattice vibrations (phonons). At first sight, scattering with longitudinal optical (LO) phonons seems to be possible only if a sublevel spacing matches the LO phonon energy $\hbar\omega_0$. In other (non-resonant) cases, scattering is expected to be impossible (or at least strongly reduced). This is the so-called phonon-bottleneck problem which has intensively been discussed in the literature.[5] The argument, however, relies on the application of Fermi's golden rule which demands energy conservation in each individual process. However, electron-phonon interaction in quantum confined systems [6, 7] gives rise to a far more complicated picture including: Non-Markovian scattering, formation of electron-phonon bound states with level repulsion, phonon satellites spaced at multiples of $\hbar\omega_0$, and

multiphonon processes in general.

The coupling of quantum dot levels to acoustic phonons is responsible for another set of features. Due to their dispersion, the possible energy transfer covers a range from zero to a maximum value (typically, a few meV) which is related to the effective dot size. Consequently, phonon satellites appear here as broad bands surrounding the zero-phonon line [8, 9]. The broadening of this line itself is a subject of intense research. In view of the phonon bottleneck problem mentioned above, one might be not surprised that an advanced theory predicts a finite broadening, even if the next confined levels are far away in energy compared to the maximum energy transfer [10].

In the present work, we want to focus on the interaction with LO phonons. This is relevant for quantum dots made from polar material like CdSe, where the Fröhlich interaction with LO phonons is much stronger than the coupling to acoustic phonons. ¿From the theoretical point of view, the dispersionless nature of the LO phonons allows a numerically exact treatment, as we have shown in calculating the electron spectral function for a GaAs dot in Ref. 11.

Král et al. [12] have dealt with the LO phonon bottleneck problem and found within a standard self energy approach (second order in the interaction) an appreciable broadening of the levels which persists even outside the exact resonance. It has further been argued that relaxation properties can be obtained from a convolution of the spectral functions of the discrete energy levels. We have derived in our previous paper [11] an efficient scheme to calculate eigenenergies and eigenvectors, which rests upon an unitary transformation of the phonons into a new set where only a few are coupled to the electronic degrees of freedom. We could show that the electron spectral function consists of a series of discrete delta functions. They are distributed around the bare level energies and at multiples of the LO energy (phonon satellites).

Under resonance conditions, the eigenenergies are still split in form of avoided level crossing. This is reminiscent to the Rabi splitting in a two-level system coupled to monochromatic photons (which formally replace the phonons). The self consistent second Born approximation for the self energy gives some gross features of the spectrum but has broadened levels instead of the closely spaced discrete lines in the exact calculation. Thus, we had concluded that this approximation fails if phonons are coupled to *discrete* electronic levels.

Looking at the influence of phonon interaction on the interband transitions, one has to refer to a seminal paper by Schmitt-Rink and coworkers [7]. They have shown that the phonon interaction in general will increase with confinement (i.e. with reducing the dot size). For the Fröhlich coupling to LO phonons, however, things are different since here the difference in charge distribution between initial (valence band sublevel) and final state (conduction band sublevel) enters. Now, under strong confinement, the sublevel wave functions are getting more close to each other. Therefore, the optical transition is accompanied with practical no change in local charge distribution, and the net LO phonon coupling is drastically reduced.

In Ref. [12], it has been claimed that the interband absorption spectrum can be taken as a convolution of the one-particle spectral functions for the electron and the hole. In the present work which extends Ref. [11] to a two-band many-level situation, and allows to calculate the linear optical response exactly, we will demonstrate the failure of this convolution approach. Indeed, it is missing the correct charge redistribution.

Recently, the absorption spectrum of individual QDs has been discussed for intra-band [13] as well as for interband transitions [14]. In the latter work, the valence band levels were treated without phonon interaction - which leads to an even simplified form of the convolution approach. In contrast, we would like to stress that the resonance condition (matching a sublevel distance by $\hbar\omega_0$) can be much easier obtained in the valence band since the sublevel spacing is here smaller than in the conduction band.

The paper is organized as follows. In section II, the model and the Hamiltonian are presented. In section III, we define and perform the unitary transformation which reduces the number of bosonic modes coupled to the fermionic states. This works if the phonons have no dispersion, and makes a numerical diagonalization of the Hamiltonian feasible. Equations for the linear polarization in terms of exact eigenstates are derived in section IV, and the approximate convolution of electron and hole spectral function is given as well. In section V, numerical results for two prototype quantum dots made from the polar material CdSe are presented and discussed. Several details on the transformations and a list of material parameters are given in the Appendix.

II. THE MODEL

We start with the standard Hamiltonian which couples the band states in a semiconductor to the lattice displacement. For the quantum dot, the confined electronic states in the conduction (valence) band are given by Fermionic operators c_j (v_j). The lattice vibrations are taken as longitudinal optical phonons without dispersion, $\hbar\omega_0$, and represented by Bosonic operators $b_{\mathbf{q}}$:

$$H = \sum_{\mathbf{q}} \hbar\omega_0 b_{\mathbf{q}}^\dagger b_{\mathbf{q}} + \sum_j \left(\epsilon_j^c c_j^\dagger c_j + \epsilon_j^v v_j^\dagger v_j \right) + \sum_{\mathbf{q}jl} \left(b_{\mathbf{q}} + b_{-\mathbf{q}}^\dagger \right) \left(M_{\mathbf{q}jl}^c c_j^\dagger c_l + M_{\mathbf{q}jl}^v v_j^\dagger v_l \right). \quad (1)$$

The coupling matrix elements $M_{\mathbf{q}jl}^a$ ($a = c, v$) stem from the Fröhlich interaction applied to the confinement wave functions (see Appendix C for details). Note that there is no phonon coupling between valence and conduction band states since the energy gap is far greater than the LO phonon energy, while the distance between confined levels in one band $\epsilon_j^a - \epsilon_l^a$ ($a = c, v$) may be well in the range of the phonon energy. Electron spin is not included here since spin relaxation is a slow process compared to the spin-conserving electron-phonon interaction. As we are focussing on the linear response, the Coulomb interaction leads to exciton formation only. Under strong confinement conditions considered here, the confinement wave functions are only reshaped marginally, and we can drop excitonic effects [15]. Similarly, phonon-assisted transitions into the continuum of wetting layer states are not considered. For simplicity, we restrict ourselves to the interaction with bulk phonon modes, leaving the more precise picture of confined and interface modes for future investigations [16].

For treating optical transitions between the filled valence band and the empty conduction band, it is convenient to switch from the conduction-valence-band description used in Eq. (1) to the electron-hole picture. This is accomplished by the replacement

$$c_j \rightarrow e_j, \quad v_j \rightarrow h_j^\dagger. \quad (2)$$

Using $v_j^\dagger v_l = \delta_{j,l} - h_l^\dagger h_j$ the Hamiltonian is rewritten as

$$H = \sum_{\mathbf{q}} \hbar\omega_0 b_{\mathbf{q}}^\dagger b_{\mathbf{q}} + \sum_j \left(\epsilon_j^c e_j^\dagger e_j - \epsilon_j^v h_j^\dagger h_j \right) + \sum_{\mathbf{q}jl} \left(b_{\mathbf{q}} + b_{-\mathbf{q}}^\dagger \right) \left(M_{\mathbf{q}jl}^c e_j^\dagger e_l - M_{\mathbf{q}jl}^v h_j^\dagger h_l \right) + \sum_j \epsilon_j^v + \sum_{\mathbf{q}j} \left(b_{\mathbf{q}} + b_{-\mathbf{q}}^\dagger \right) M_{\mathbf{q}jj}^v. \quad (3)$$

Note that the phonon interaction carries now a negative sign for the hole states compared to the electron states, which can be traced back to the different charge sign of both excitations. In Appendix A we show that the last line can be dropped by renormalizing the ground state energy.

III. REDUCING THE PHONON SUBSPACE

We observe that the phonon coupling in Eq. (3) involves only certain combinations of phonon operators, e.g. $\sum_{\mathbf{q}} M_{\mathbf{q}jl}^c b_{\mathbf{q}}$. If we consider a finite number (say m) of electron sublevels in the dot, and m hole sublevels as well, there are $2m^2$ such combinations (as argued above, phonon-assisted transitions between conduction and valence bands are absent). However, since we can take *real* confinement wave functions, the symmetry $M_{\mathbf{q}lj}^a = M_{\mathbf{q}jl}^a$ holds. This reduces the linear independent combinations to $m(m+1)$.

A further reduction can be achieved since in the present Hamiltonian Eq. (3), the number of electrons (N_e) and of holes (N_h) are conserved quantities. Therefore, two (diagonal) Fermion pairs in the interaction can be expressed by the remaining ones. We choose

$$e_m^\dagger e_m = N_e - \sum_{j=1}^{m-1} e_j^\dagger e_j, \quad h_m^\dagger h_m = N_h - \sum_{j=1}^{m-1} h_j^\dagger h_j, \quad (4)$$

which gives additions to all the other diagonal coupling terms, and a c number remainder. In order to shorten the subsequent writing, we introduce pair indices $\lambda = 1, \dots, (m(m+1)-2)$ which combine either two electron sublevels ($e;jl$) or two hole sublevels ($h;jl$), with $j \geq l$. Caring for the different signs in the interaction of Eq. (3), we define in the conduction band

$$M_{\mathbf{q}\lambda} = M_{\mathbf{q}jl}^c - \delta_{jl} M_{\mathbf{q}mm}^c, \quad (5)$$

and in the valence band

$$M_{\mathbf{q}\lambda} = -M_{\mathbf{q}lj}^v + \delta_{jl} M_{\mathbf{q}mm}^v. \quad (6)$$

For treating the c number part properly, we have to introduce one further index $\lambda = \kappa \equiv m(m+1)-1$, with the matrix element

$$M_{\mathbf{q}\kappa} = N_e M_{\mathbf{q}mm}^c - N_h M_{\mathbf{q}mm}^v. \quad (7)$$

Now, the interaction term of Eq. (3) reads

$$\sum_{\lambda=1}^{\kappa-1} \left(A_\lambda + A_\lambda^\dagger \right) (c^\dagger c)_\lambda + (A_\kappa + A_\kappa^\dagger) \quad (8)$$

with a shorthand writing for the fermionic operators. Note that for the nondiagonal terms $j \neq l$, we have to set e.g.

$$(c^\dagger c)_\lambda = e_j^\dagger e_l + e_l^\dagger e_j. \quad (9)$$

The combinations of phonon operators entering Eq. (8) are

$$A_\lambda = \sum_{\mathbf{q}} M_{\mathbf{q}\lambda} b_{\mathbf{q}} \quad (\lambda = 1 \dots \kappa), \quad (10)$$

but the A_λ do not form an orthonormal set. As detailed in Appendix B, we apply the Gram-Schmidt orthonormalization scheme to generate new phonon operators B_λ

which are properly orthogonalized. The transformation is a linear one,

$$A_\lambda = \sum_{\alpha=1}^{\lambda} I_{\lambda\alpha} B_\alpha, \quad (11)$$

and leads to the transformed Hamiltonian

$$\begin{aligned} H = & \sum_{\lambda} \hbar\omega_0 B_\lambda^\dagger B_\lambda + \sum_j \left(\epsilon_j^c e_j^\dagger e_j - \epsilon_j^v h_j^\dagger h_j \right) \\ & + \sum_{\lambda=1}^{\kappa-1} \sum_{\alpha=1}^{\lambda} \left(I_{\lambda\alpha} B_\alpha + I_{\lambda\alpha}^* B_\alpha^\dagger \right) (c^\dagger c)_\lambda \\ & + \sum_{\alpha=1}^{\kappa} \left(I_{\kappa\alpha} B_\alpha + I_{\kappa\alpha}^* B_\alpha^\dagger \right). \end{aligned} \quad (12)$$

For arriving at the standard diagonal form of the free phonon part, it was essential that the phonons have no dispersion. Otherwise, the subset of B_λ would still mix with the remaining phonon operators. These remaining degrees of freedom contribute only to the free phonon energy and are omitted from Eq. (12).

A careful inspection of Eq. (12) shows that the Bosonic operator B_κ only appears as last element in the last line of Eq. (12), and in the free phonon part. It is therefore decoupled from the Hamiltonian and allows an independent solution in terms of a shifted oscillator,

$$\mathcal{B}_\kappa = B_\kappa + I_{\kappa\kappa}/\hbar\omega_0. \quad (13)$$

Therefore, only $(m(m+1)-2)$ new modes are coupled to the Fermionic Hilbert space.

Assuming a symmetric dot shape, the confinement functions are either even or odd, and the matrix elements $M_{\mathbf{q}jl}^a$ have a definite parity in \mathbf{q} , too. Consequently, the compound matrix elements $M_{\lambda\alpha}$ defined in Eq. (B5) vanish if λ and α refer to different parity. Therefore, the tridiagonal matrix K (and I as well) has a block structure, allowing the Gram-Schmidt procedure to work in each block independently.

IV. LINEAR OPTICAL RESPONSE

In this section, we want to contrast the direct evaluation of the time-dependent linear polarization and the absorption spectrum with the so-called *convolution approach*: Here, only the spectral functions of the electron and hole states are calculated, and the absorption is taken as a convolution of both quantities. Before deriving the corresponding formal expressions, let us point out the main difference: For the direct evaluation, we start from the electron-hole vacuum ($N_e = 0, N_h = 0$) as initial state and end up in the subspace of one electron-hole pair ($N_e = 1, N_h = 1$). For the convolution approach, quite different subspaces are invoked, namely $N_e = 0, N_h = 0 \rightarrow N_e = 1, N_h = 0$ for the electron spectral function, and $N_e = 0, N_h = 0 \rightarrow N_e = 0, N_h = 1$

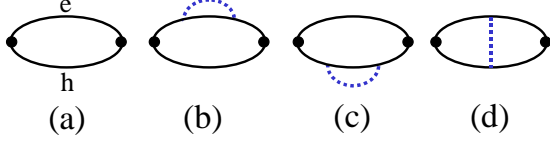


FIG. 1: Diagrammatic expansion of the optical polarization up to first order in the electron-phonon interaction. Lines denote the electron (e) and hole (h) propagator, the dotted line the phonon propagator, and the large dot stands for the optical dipole matrix element. The zeroth-order diagram (a) describes interband transitions between confined states unaffected by the phonon interaction. In the convolution approach, only self-energy type diagrams (b, c) are considered, while in the full evaluation, vertex type diagrams (d) are included as well.

for the hole one. In diagram language, any process which has a phonon correlation between electron and hole levels is discarded in the convolution approach. In Fig. 1, we display the relevant first order diagrams. The vertex diagram Fig. 1d is the first one describing interband phonon correlations. In particular under strong confinement conditions, it compensates to a large extent the self-energy type diagrams (Fig. 1b, c). Only the latter are kept in the convolution approach, and we expect much to strong phonon satellites in this approximate treatment. Formally, in the convolution approach, the matrix elements appear as $(M^c)^2$ or $(M^v)^2$, while the full version includes the vertex corrections containing $M_c M_v$ as well. For level-diagonal matrix elements, this combines into $(M^c - M^v)^2$. The appearance of matrix element differences can be seen already in Eq. (3). Therefore, the near cancellation of changes in the charge distribution [7] can only be achieved when treating self energy and vertex diagrams on an equal footing.

A. Direct evaluation

The coupling to the light is described within the dipole approximation for interband transitions, adding

$$E(t) \sum_{ij} (\mu_{ij} c_i^\dagger v_j + h.c.) \quad (14)$$

as a perturbation to the Hamiltonian. The dipole matrix elements are given by an integral over the confinement functions,

$$\mu_{ij} = \mu_{cv} \int d^3r \psi_i^e(\mathbf{r}) \psi_j^h(\mathbf{r}), \quad (15)$$

having as prefactor the dipole moment between the valence and conduction band, μ_{cv} .

The linear optical response follows from the polarization after a unit-area delta pulse at $t = 0$ and is given

as dipole-dipole-correlation function. Expressed via the electron and hole operators, we have for $t \geq 0$

$$P(t) = i \sum_{ij,kl} \mu_{kl}^* \mu_{ij} \langle h_l(t) e_k(t) e_i^\dagger(0) h_j^\dagger(0) \rangle \quad (16)$$

with the time dependence of the operators in the Heisenberg picture. The expectation value is shorthand writing for the statistical sum over initial states which contain no electron-hole pairs, and a thermal distribution of phonon mode occupations $n_\lambda = 0, 1, \dots, \infty$. This is denoted by $|n_\lambda, 0\rangle$, with total energy

$$E_0 = \hbar\omega_0 \sum_\lambda n_\lambda. \quad (17)$$

Then, we proceed with

$$P(t) \propto i \sum_{n_\lambda} e^{-\beta E_0} \sum_{ij,kl} \mu_{kl}^* \mu_{ij} \langle n_\lambda, 0 | h_l(t) e_k(t) | n_\lambda, ij \rangle. \quad (18)$$

In practice, the independent summation over phonon occupations n_λ can be restricted to a maximum number which depends on coupling strength and temperature, $\beta = 1/k_B T$. For simplicity, we have omitted a prefactor which ensures the proper normalization of the statistical sum.

While the zero-pair states $|n_\lambda, 0\rangle$ diagonalize the zero-pair Hamiltonian properly, we need to look for the one-pair states from the eigenvalue problem

$$H_1 |\phi\rangle = E_\phi |\phi\rangle. \quad (19)$$

Due to the reduction of the number of Bosonic modes, this can be solved numerically exact by expanding into the noninteracting one-pair basis $|n_\lambda, ij\rangle$.

Plugging all time dependencies together, we obtain

$$P(t) = i \sum_{n_\lambda} e^{-\beta E_0} \sum_{ij,kl,\phi} \mu_{kl} \mu_{ij} \times e^{i(E_0 - E_\phi)t/\hbar} \langle n_\lambda, kl | \phi \rangle \langle \phi | n_\lambda, ij \rangle. \quad (20)$$

Starting with the initial value

$$P(t=0) = i \sum_{n_\lambda} e^{-\beta E_0} \sum_{kl} |\mu_{kl}|^2, \quad (21)$$

the polarization evolves in time as a sum over many individual oscillations. Although each of these terms does not have a damping, in the sum a general decay can be observed (quasi-dephasing), as shown in Sec. V.

The imaginary part of the Fourier transformation of the polarization function yields the absorption spectrum,

$$\begin{aligned} \alpha(\omega) &= \text{Im} \int_{-\infty}^{\infty} dt P(t) e^{i\omega t} \\ &\propto \sum_{n_\lambda} e^{-\beta E_0} \sum_{ij,kl,\phi} \mu_{kl}^* \mu_{ij} \\ &\times \langle n_\lambda, kl | \phi \rangle \langle \phi | n_\lambda, ij \rangle \delta(E_\phi - E_0 - \hbar\omega). \end{aligned} \quad (22)$$

$$\times \langle n_\lambda, kl | \phi \rangle \langle \phi | n_\lambda, ij \rangle \delta(E_\phi - E_0 - \hbar\omega). \quad (23)$$

Let us point out that the exact absorption spectrum consists of delta peaks only. This was clear from the beginning since a finite perturbation cannot change the character of the spectrum of the unperturbed system. Since we started from *dispersionless* Bosonic modes, the discrete electronic spectrum cannot be altered by the non-zero electron-phonon interaction [17].

B. Convolution approach

It has been argued at several places in the literature [12], that the convolution of electron and hole spectral functions $\alpha^C(\omega)$ may give a reasonable approximation to the absorption spectrum,

$$\alpha^C(\omega) \propto \int d\omega' \sum_{ij,kl} \mu_{kl}^* \mu_{ij} A_{ki}^e(\omega') A_{lj}^h(\omega - \omega'). \quad (24)$$

For the specific form of the frequency convolution, note that the hole spectral functions has delta peaks around $-\epsilon_l^v$, while the electron one peaks at $+\epsilon_k^c$. Indeed, avoiding the evaluation of the two-particle (i.e. dipole-dipole) correlation functions would be an important reduction of the numerical labor, since the spectral function is a genuine one-particle function. We concentrate on the electron spectral function $A_{ki}^e(\omega)$ which is defined by

$$A_{ki}^e(\omega) = \frac{1}{\pi} \text{Re} \int_0^\infty dt e^{i\omega t} \langle e_k(t) e_i^\dagger(0) \rangle. \quad (25)$$

Here, we need the exact eigenstates of the Hilbert space with $N_e = 1$, $N_h = 0$ which will be denoted by $H_e|\chi\rangle = E_\chi|\chi\rangle$. Similar arguments as used in deriving Eq. (20) lead to

$$A_{ki}^e(\omega) \propto \sum_{n_\lambda} e^{-\beta E_0} \times \sum_{\chi} \langle n_\lambda, k | \chi \rangle \langle \chi | n_\lambda, i \rangle \delta(E_\chi - E_0 - \hbar\omega), \quad (26)$$

where $|n_\lambda, k\rangle$ is the (non-interacting) one-electron basis. In general, the spectral function including phonon interaction forms a matrix in electron sublevel space. In the present case, however, the well-defined parity of the two electron states under consideration leads to $A_{ki}^e \propto \delta_{ki}$. Similar equations hold for the hole spectral function.

V. NUMERICAL RESULTS

We consider a prototype quantum dot of ellipsoidal shape with CdSe as the semiconductor material. The relevant LO phonon energy is $\hbar\omega_0 = 24 \text{ meV}$, and we consider the two lowest confined states in the conduction and in the valence band ($m = 2$). In total, we have $m(m+1) - 2 = 4$ new phonon modes. According to what has been said before, there is the odd parity group

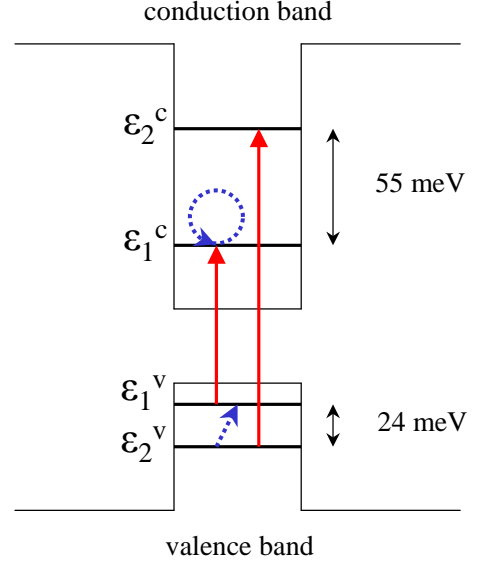


FIG. 2: Schematic band diagram with sublevel spacings corresponding to the resonant quantum dot. Vertical arrows - optical transitions, dotted lines - phonon processes. For further explanations, see text.

($\lambda = \text{e:12, h:12}$) and the even parity group ($\lambda = \text{e:11, h:11}$). The special mode $\lambda = \kappa \equiv 5$ refers to the even parity group. Consequently, K and I decompose into a two-dimensional and a three-dimensional block. In the sequel, we calculate the linear optical properties for two different dot sizes. One has perfect resonance between phonon energy and sublevel distance in the valence band (*resonant quantum dot*), $\Delta^v = \hbar\omega_0 = 24 \text{ meV}$ and $\Delta^c = 55 \text{ meV}$. Sublevel distances (without phonon interaction) are defined as

$$\Delta^a \equiv |\epsilon_2^a - \epsilon_1^a| \quad (a = c, v). \quad (27)$$

In Fig. 2, the confinement levels for the resonant QD are shown schematically. Vertical arrows mark the nonzero optical transitions. The dotted lines denote phonon processes. In the valence band, this is resonant with the sublevel distance (real transition, driven by $M_{\mathbf{q}12}^v$). In the conduction band, a virtual process involving the diagonal matrix element $M_{\mathbf{q}11}^c$ is depicted.

The second choice is backed by experimentally measured level distances from Refs. [4, 18] and comes out to be a *non-resonant quantum dot* with $\Delta^v = 35 \text{ meV}$ and $\Delta^c = 80 \text{ meV}$. More details on the extraction of size parameters are given in Appendix D.

A. Direct evaluation

To determine the full linear response, we need to solve the eigenvalue problem for the one-pair subspace Eq. (19). As mentioned at the end of Sec. II, it will consist of four fermionic states which are coupled to four

Bosonic modes. We truncate the Hilbert space by only considering states where the sum of the occupation numbers of all four modes is not larger than 10. This gives 1001 different Bosonic states using the binomial coefficient (14 over 4). For the Fermionic states $|jl\rangle$, we can exploit an additional parity symmetry: Due to the operator form Eq. (9) in the phonon interaction of Eq. (12), the combinations

$$\frac{1}{\sqrt{2}}(|11\rangle + |22\rangle), \quad \frac{1}{\sqrt{2}}(|12\rangle + |21\rangle) \quad (28)$$

are decoupled from the corresponding set with minus signs. Thus, in total, two matrices with 2002×2002 elements each have to be diagonalized. At $T = 77$ K, we have $\beta\hbar\omega_0 = 3.62$, which tells us that LO phonon emission processes are dominant. By checking the convergency, we found that the first 200 eigenvalues are sufficient to describe the spectra properly.

In dealing with the special phonon mode B_5 , we have to evaluate the matrix elements between the unshifted oscillator (in the initial state) and the shifted one (in the final state),

$$\langle n, 0 | n', s \rangle = e^{-s^2/2} \sum_{k=0}^{\min(n, n')} \frac{(-1)^{k+n} \sqrt{n!n'!}}{k!(n-k)!(n'-k)!} s^{n+n'-2k}. \quad (29)$$

The shift parameter is given as second argument in the state, here $s = I_{55}/\hbar\omega_0$. In the polarization, this part gives rise to an additional factor of

$$\sum_{n_5, n'_5} e^{-\beta n_5 \hbar \omega_0} e^{i(n_5 - n'_5 - s^2)\omega_0 t} |\langle n_5, 0 | n'_5, s \rangle|^2. \quad (30)$$

Note the appearance of s^2 as a correction to the final state energy. For the absorption spectrum, first the spectrum without the special mode is calculated, and subsequently spectrally displaced and added up, as the Fourier transform of Eq. (30) dictates.

The temporal decay of the polarization amplitude $|P(t)|$ is displayed in Figs. 3 for the resonant QD. In the calculation, we have taken into account only transitions which are energetically close to the $h1 \rightarrow e1$ transition. Thus, phonon satellites and the interference with the other main transition $h2 \rightarrow e2$ are suppressed. This spectral window would correspond to a finite-duration excitation pulse spectrally centered around $\epsilon_1^c - \epsilon_1^v$. For an elevated temperature of 300 K, the initial decay goes faster, which resembles a traditional temperature-dependent dephasing. However, at larger times, the polarization oscillates irregularly around a finite value (therefore, we would like to use the term *quasi-dephasing*).

For the absorption spectrum, we have chosen to broaden all discrete lines in Eq. (22) with a Gaussian of variance $\sigma = 1$ meV. In this way, we achieve to visualize both, the transition energies and their oscillator strengths.

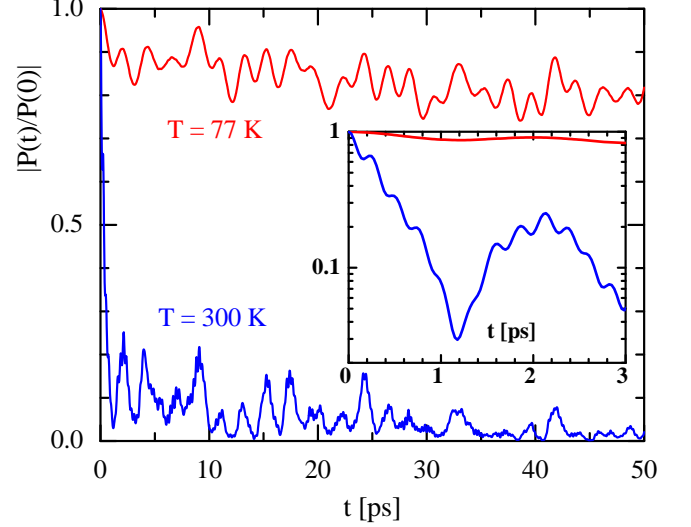


FIG. 3: Temporal decay of the linear polarization for the resonant QD at $T = 77$ K. (upper curve) and $T = 300$ K (lower curve). The excitation pulse is centered around the lower transition $h1 \rightarrow e1$ with a spectral window of ± 12 meV. The inset shows the initial decay on a logarithmic scale.

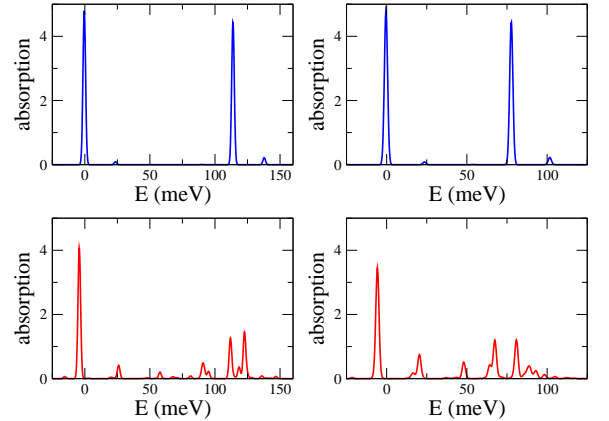


FIG. 4: Normalized absorption spectrum $\alpha(\omega)$ for the non-resonant QD (left) and the resonant QD (right) at $T = 77$ K. The lower panels refer to the full model while the upper panels are restricted to level-diagonal phonon coupling. The bare $h1 \rightarrow e1$ transition energy is chosen as zero of energy.

In Fig. 4, the normalized absorption spectrum $\alpha(\omega)$ is shown for both the non-resonant QD (left) and the resonant one (right). In both cases, the curves in the lower panels are calculated with all phonon couplings present. A set of closely spaced levels (bundle) is seen around the two optically allowed (bare) transitions $h1 \rightarrow e1$ and $h2 \rightarrow e2$. The excited-state bundle for the resonant QD exhibits a particular broad range, which is the spectral counterpart of the decay seen in the time-resolved polarization. A simple theory like e.g. the second Born

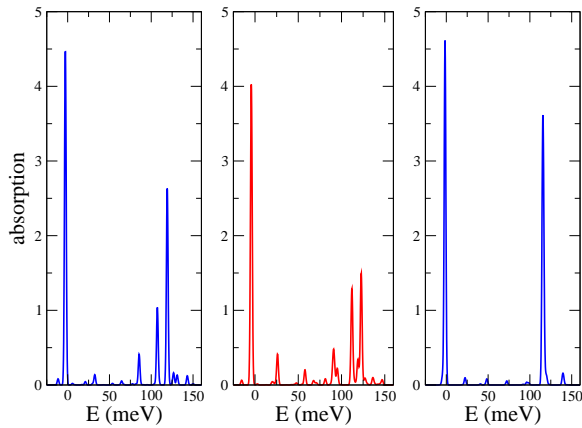


FIG. 5: Normalized absorption spectrum $\alpha(\omega)$ for the non-resonant QD at $T = 77$ K. (a) calculated without non-diagonal electron coupling, (b) all couplings included, (c) without non-diagonal hole coupling.

approximation [12] would here produce a real broadening of the line, which may be related to a real dephasing process via energy-conserving phonon emission. We see that in the present exact treatment, the situation is a bit more complex, and can at best be called quasi-dephasing. Also, the comparison with the non-resonant dot (left) shows that quasi-dephasing is in no way restricted to exact resonance. In our opinion, this explains the absence of a clear phonon bottleneck in polar quantum dots.

Further, small lines can be identified as phonon satellites, which are located at multiples of $\hbar\omega_0$ with respect to the main lines. Comparing the energetic position of the $h1 \rightarrow e1$ main line with its bare energy $\epsilon_1^c - \epsilon_2^v$, we can extract polaron shifts of the QD. For the non-resonant QD we found a value of 4 meV. The standard expression for the polaron shift in bulk CdSe gives 11.3 meV (21.1 meV) for electrons (holes), respectively, being much larger than the shift in our QD calculation. This shows indeed the strong charge cancellation in a QD as discussed in Ref. [7]. In addition, the restriction to two sublevels in each band might underestimate our calculated QD polaron shift.

We have also calculated the spectrum for the reduced model of level-diagonal phonon coupling $M_{\mathbf{q}ij}^a \propto \delta_{ij}$ (upper panels in Fig. 4). This case is known to be exactly solvable and called *Independent Boson Model*, see Ref. [19]. We found excellent agreement supporting our method, and could justify the chosen truncation in Boson occupation. The level-diagonal absorption spectrum exhibits phonon satellites which carry only a few percent of the total weight, leaving the zero phonon line as the dominant feature. The inclusion of the intra-level coupling thus changes the absorption spectrum significantly, in particular for the resonant QD.

Fig. 5 illustrates the importance of nondiagonal phonon coupling included for electrons or holes separately. The upper panel contains the absorption spectrum with diagonal coupling for electrons, $M_{\mathbf{q}12}^c = 0$,

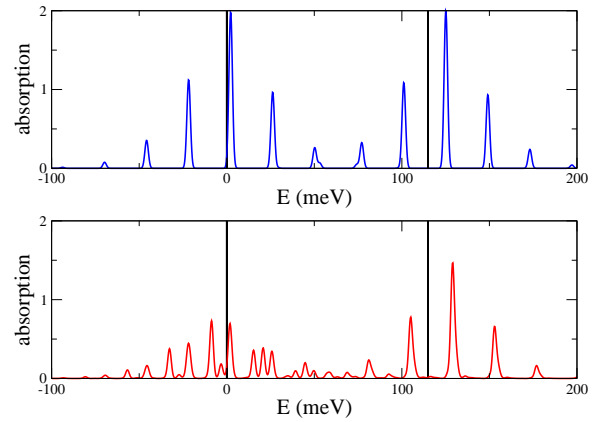


FIG. 6: Normalized absorption spectrum $\alpha^C(\omega)$ obtained from convoluting the spectral functions for the non-resonant QD. The transition energies without phonon interaction are shown as vertical markers. The upper panel refers to the diagonal coupling, while the lower panel includes all coupling matrix elements.

but full coupling for the holes. Vice versa, the lower panel displays the hole diagonal case. For comparison, the absorption spectrum of the full model is shown in the middle panel.

B. Convolution approach

Performing the unitary transformation described in section III on the Hamiltonian for each band separately, we end up with a model containing three Bosonic modes. Using the conservation of the electron (hole) number, we finally have to diagonalize a Hamiltonian with two Bosonic modes and two fermionic states each. This has been discussed at length in our previous paper Ref. [11].

In Figure 6, the absorption spectrum $\alpha^C(\omega)$ stemming from the convolution of the spectral functions Eq. (24) is shown for the non-resonant case. In order to reach the same artificial broadening of the absorption spectrum, we have to broaden the spectral functions with a Gaussian of reduced variance, $\sigma = 1/\sqrt{2}$ meV. The inclusion of nondiagonal matrix elements (lower panel) is not so important here, as the spectrum is dominated by strong phonon satellites. A comparison with the exact spectrum of Fig. 4 (bottom left) shows, however, that these satellites are much too strong. As discussed at the beginning of Sec. IV, it is the correlated phonon scattering between electron and hole states which reduces the satellite structure appreciably. Thus, the one-particle spectral functions are insufficient to describe the optical transitions. We conclude therefore that the convolution approach as applied in Refs. [12, 14] has to be abandoned, even if the phonon coupling is of moderate strength, as in the present example.

VI. SUMMARY

We have presented a solvable model which serves to describe linear optical properties of a single quantum dot interacting with LO phonons. The linear polarization and the corresponding absorption spectrum is calculated by diagonalizing the appropriate Hilbert space of four electronic levels and four Bosonic modes split off from the full phonon modes via an orthogonalization procedure. The correct evaluation of the two-particle dipole-dipole correlation function is contrasted with a simplified approach using the spectral convolution of one-particle spectral functions. The numerics shows this convolution approach to be inadequate, in particular it produces phonon satellites strongly enhanced compared to the correct result. Qualitatively, this can be traced back to a missing compensation between different contributions in a diagrammatic analysis.

Parameter values for CdSe QDs are used, and a comparison between resonant and non-resonant QDs is carried out. Signatures of the phonon bottleneck are found, i.e. a stronger quasi-dephasing for the resonant case, but this is not as dramatic as simple arguments using Fermi's golden rule for phonon emission would predict.

VII. ACKNOWLEDGMENTS

Funding from MCyT (Spain) through grant MAT2002-04095-C02-01 and from DFG (Germany) through Sfb 296 is acknowledged.

APPENDIX A: ELECTRON-HOLE TRANSFORMATION

Switching from the conduction-valence-band description to the electron-hole picture produces a shift in the Bosonic operators. Here we show that only the shift of the zero-momentum mode survives.

To proceed we have to use the complete form of the confinement wave function including the Wannier basis $w_a(\mathbf{r})$ of the band under consideration,

$$\Psi_j^a(\mathbf{r}) = \sum_{\mathbf{R}} \psi_{j\mathbf{R}}^a w_a(\mathbf{r} - \mathbf{R}), \quad (\text{A1})$$

where $\psi_{j\mathbf{R}}^a$ is the envelope part (called confinement function in the previous sections). The orthogonality of the (real) wave functions induces

$$\delta_{jl} = \int_{\Omega} d^3r \Psi_j^a(\mathbf{r}) \Psi_l^a(\mathbf{r}) = \sum_{\mathbf{R}} \psi_{j\mathbf{R}}^a \psi_{l\mathbf{R}}^a, \quad (\text{A2})$$

since the Wannier functions are orthogonal on different

lattice sites $\mathbf{R} \neq \mathbf{R}'$. Dropping prefactors, we evaluate

$$\begin{aligned} \sum_j M_{\mathbf{q}jj}^a &\propto \int_{\Omega} d^3r \sum_{\mathbf{R}\mathbf{R}'j} \psi_{j\mathbf{R}}^a \psi_{j\mathbf{R}'}^a e^{i\mathbf{q}\mathbf{r}} \\ &\times w_a(\mathbf{r} - \mathbf{R}) w_a(\mathbf{r} - \mathbf{R}') \equiv C_{\mathbf{q}}. \end{aligned} \quad (\text{A3})$$

The sum over j gives a Kronecker symbol $\delta_{\mathbf{R}\mathbf{R}'}$ due to the completeness of the coefficients $\psi_{j\mathbf{R}}^a$. The remaining integral simplifies to

$$\begin{aligned} C_{\mathbf{q}} &= \int_{\Omega} d^3r \sum_{\mathbf{R}} e^{i\mathbf{q}\mathbf{r}} w_a^2(\mathbf{r} - \mathbf{R}) \\ &= \int_{\Omega} d^3r' e^{i\mathbf{q}\mathbf{r}'} w_a^2(\mathbf{r}') \sum_{\mathbf{R}} e^{i\mathbf{q}\mathbf{R}}. \end{aligned} \quad (\text{A4})$$

The last sum over \mathbf{R} produces $\mathcal{N}\delta_{\mathbf{q}0}$, where \mathcal{N} is the number of elementary cells Ω_0 within the normalization volume, $\Omega = \mathcal{N}\Omega_0$. Altogether we have

$$C_{\mathbf{q}} = \delta_{\mathbf{q}0} \mathcal{N}. \quad (\text{A5})$$

Therefore, the correction in the last line of Eq. (3) reduces to zero momentum,

$$\begin{aligned} &(b_0^\dagger + b_0) \sqrt{\mathcal{N}\hbar\omega_0} \alpha_v(q), \\ \alpha_v(q) &= \sqrt{\frac{1}{\Omega_0} \frac{e^2}{2q^2} \left(\frac{1}{\varepsilon_\infty} - \frac{1}{\varepsilon_S} \right)}. \end{aligned} \quad (\text{A6})$$

In the prefactor $\alpha_v(q)$, we let $q \rightarrow 0$ at the end.

In order to remove the last line from the Hamiltonian, the zero-momentum phonon operator is shifted according to

$$b_0 + \alpha_v(q) \sqrt{\mathcal{N}/\hbar\omega_0} \rightarrow b_0, \quad (\text{A7})$$

which brings from the free phonon Hamiltonian a quadratic contribution $\mathcal{N}\alpha_v^2(q)$. Together with the valence energy sum, this gives an unimportant c number contribution which can be dropped. However, the electron-phonon interaction is getting an addition at $\mathbf{q} \rightarrow 0$, too. Due to the orthogonality of the confinement functions, we have in leading order

$$M_{\mathbf{q}jl}^a = \sqrt{\frac{\hbar\omega_0}{\mathcal{N}}} \alpha_v(q) (\delta_{jl} + O(q)), \quad (\text{A8})$$

which gives as correction

$$-2\alpha_v^2(q) (e_i^\dagger e_i - h_i^\dagger h_i). \quad (\text{A9})$$

However, this term vanishes for any state having no or an equal number of electrons and holes (charge neutrality). For optical excitation and recombination, this is just the relevant sector of the Hilbert space. Therefore, the singularity in $\alpha_v(q) \propto 1/q$ (which would have to be treated carefully) does not contribute to physical quantities.

Finally, we note that the above argument also holds for acoustic phonons.

APPENDIX B: GRAM-SCHMIDT ORTHONORMALIZATION

We apply the Gram-Schmidt scheme by first constructing the orthogonal operator set

$$\tilde{B}_1 = A_1, \quad \tilde{B}_\lambda = A_\lambda - \sum_{\alpha=1}^{\lambda-1} [A_\lambda, B_\alpha^\dagger] B_\alpha, \quad (\text{B1})$$

and normalizing it afterwards via

$$B_\lambda = N_\lambda \tilde{B}_\lambda \quad \text{where} \quad N_\lambda^{-2} = [\tilde{B}_\lambda, \tilde{B}_\lambda^\dagger]. \quad (\text{B2})$$

The new operators obey the canonical commutation rules

$$[B_\lambda, B_\alpha^\dagger] = \delta_{\lambda\alpha}. \quad (\text{B3})$$

The final result can be written as a linear transformation

$$B_\lambda = N_\lambda \sum_{\alpha=1}^{\lambda} K_{\lambda\alpha} A_\alpha. \quad (\text{B4})$$

By construction, $K_{\lambda\alpha}$ is a tridiagonal matrix which has nonzero elements for $\lambda \geq \alpha$ only. The key ingredient for its evaluation is the commutator

$$\begin{aligned} [A_\lambda, A_\alpha^\dagger] &= \sum_{\mathbf{q}\mathbf{q}'} M_{\mathbf{q}\lambda} M_{\mathbf{q}'\alpha}^* [b_{\mathbf{q}}, b_{\mathbf{q}'}^\dagger] \\ &= \sum_{\mathbf{q}} M_{\mathbf{q}\lambda} M_{\mathbf{q}\alpha}^* \equiv M_{\lambda\alpha}, \end{aligned} \quad (\text{B5})$$

and we get a recursive determination according to

$$\begin{aligned} K_{\lambda\lambda} &= 1, \\ K_{\lambda\alpha} &= - \sum_{\beta=\alpha}^{\lambda-1} N_\beta^2 K_{\beta\alpha} \sum_{\nu=1}^{\beta} M_{\lambda\nu} K_{\beta\nu}^* \quad (\lambda > \alpha). \end{aligned} \quad (\text{B6})$$

The norm follows from

$$N_\lambda^{-2} = \sum_{\alpha,\beta=1}^{\lambda} K_{\lambda\alpha} M_{\alpha\beta} K_{\lambda\beta}^*. \quad (\text{B7})$$

In order to transform the Hamilton operator to the new phonon operators B_λ , we need to invert Eq. (B4),

$$A_\lambda = \sum_{\alpha=1}^{\lambda} I_{\lambda\alpha} B_\alpha. \quad (\text{B8})$$

Again, I is tridiagonal and can be determined quite easily via

$$I_{\lambda\lambda} = 1/N_\lambda, \quad \lambda > \alpha : I_{\lambda\alpha} = - \sum_{\beta=\alpha}^{\lambda-1} K_{\lambda\beta} I_{\beta\alpha}. \quad (\text{B9})$$

APPENDIX C: COUPLING MATRIX ELEMENTS

The standard Fröhlich coupling for the electron-LO-phonon interaction is applied to the dot confinement states,

$$\begin{aligned} M_{\mathbf{q}j\ell}^a &= \sqrt{\frac{\hbar\omega_0}{\Omega} \frac{e^2}{2q^2} \left(\frac{1}{\varepsilon_\infty} - \frac{1}{\varepsilon_S} \right)} \Phi_{\mathbf{q}j\ell}^a, \\ \Phi_{\mathbf{q}j\ell}^a &= \int d^3r \psi_j^a(\mathbf{r}) e^{i\mathbf{q}\cdot\mathbf{r}} \psi_\ell^a(\mathbf{r}) \quad (a = c, v) \end{aligned} \quad (\text{C1})$$

. For simplicity we consider an anisotropic parabolic potential as dot confinement for both, electrons and holes, with x as the long axis. The two energetically lowest wave functions are given by

$$\begin{aligned} \psi_1^a(\mathbf{r}) &= \frac{1}{N_0} \exp -\frac{1}{2} \left(\frac{x^2}{X_a^2} + \frac{y^2}{Y_a^2} + \frac{z^2}{Z_a^2} \right), \\ \psi_2^a(\mathbf{r}) &= \sqrt{2} \frac{x}{X_a} \psi_1^a(\mathbf{r}), \end{aligned} \quad (\text{C2})$$

where $X_a > Y_a, Z_a$ are the spatial extensions (variances) of the ground state, and $N_0^2 = \pi^{3/2} X_a Y_a Z_a$ its normalization.

The matrix elements in Eq. (C1) thus read

$$\begin{aligned} \Phi_{\mathbf{q}11}^a &= \exp \left(-\frac{1}{4} (q_x^2 X_a^2 + q_y^2 Y_a^2 + q_z^2 Z_a^2) \right), \\ \Phi_{\mathbf{q}21}^a &= i q_x X_a / \sqrt{2} \Phi_{\mathbf{q}11}^a, \\ \Phi_{\mathbf{q}22}^a &= (1 - q_x^2 X_a^2 / 2) \Phi_{\mathbf{q}11}^a. \end{aligned} \quad (\text{C3})$$

As described in section III, the new coupling constants are obtained by integrating a pair of coupling constants $M_{\mathbf{q}ij}^a$ over \mathbf{q} . This final integration can be reduced to the following (elliptic) integrals,

$$J_n = \int_1^\infty dt \frac{t^{-n}}{\sqrt{t(t-p)(t-q)}} \quad (n = 0, 1, 2) \quad (\text{C4})$$

with $p = 1 - (Y_a^2 + Y_b^2)/(X_a^2 + X_b^2) < 1$ and $q = 1 - (Z_a^2 + Z_b^2)/(X_a^2 + X_b^2) < 1$. For a cylindrically symmetric potential with $Y_a = Z_a$, we have $p = q$, and the integrals reduce to simple analytic functions,

$$J_0 = \frac{1}{\sqrt{p}} \log \frac{1 + \sqrt{p}}{1 - \sqrt{p}}, \quad J_1 = \frac{J_0 - 2}{p}, \quad J_2 = \frac{J_1 - 2/3}{p}.$$

APPENDIX D: MATERIAL PARAMETERS

In the calculation, parameter values for the polar semiconductor material CdSe forming the quantum dot are needed. In particular, we have taken from Ref. [20]: LO-phonon energy $\hbar\omega_0 = 24$ meV, conduction band mass $m_c = 0.13 m_0$, valence band mass $m_v = 0.45 m_0$; and dielectric constants from Ref. [21]: $\varepsilon_S = 9.57$, $\varepsilon_\infty = 6.27$.

We assume that the confinement potentials of electrons and holes are scaled by a fixed ratio ρ which is given

by the ratio between conduction band offset and valence band offset for barrier (ZnSe) and dot material (CdSe), $\rho = 5.44$ [20]. Applying this to the parabolic potential, we find a unique ratio between the lengths in the oscillator eigenfunctions Eq. (C2),

$$\xi \equiv \frac{L_c}{L_v} = \left(\frac{m_v}{m_c \rho} \right)^{1/4}, \quad (L = X, Y, Z) \quad (\text{D1})$$

which equals $\xi = 0.89$.

Since the x direction is taken as the longest one, the energetic distance between ground level ($j = 1$) and first excited level ($j = 2$) is exclusively given by the x -confinement,

$$\Delta^a \equiv |\epsilon_2^a - \epsilon_1^a| = \frac{\hbar^2}{m_a X_a^2} \quad (a = c, v). \quad (\text{D2})$$

Taking experimental values which have been reported for a certain CdSe quantum dot in Refs. [4, 18] ($\Delta^c = 80$ meV, $\Delta^v = 35$ meV) we obtain according to Eq. (D2) $X_c = 2.71$ nm and $X_v = 2.20$ nm. This yields a length ratio of $\xi = X_c/X_v = 1.23$ which is larger than the value derived from Eq. (D1). However, a possible alloying of the QD material [16] and the assumed parabolic confinement potential may introduce substantial uncertainties. In the numerical calculations, we have used $\xi = 1.23$ throughout. There is no direct access to the size of the QD in the other (shorter) directions. To

keep things simple, we take the same representative value for the two smaller lengths: $Y_v = Z_v = 2.00$ nm and $Y_c = Z_c = \xi Y_v = 2.46$ nm.

It is easily seen from the parity of the oscillator wave functions Eq. (C2), that the optical transitions $h1 \rightarrow e2$ and $h2 \rightarrow e1$ are forbidden. The remaining non-zero dipole matrix elements Eq. (15) can be expressed by the same length ratio ξ introduced above. In units of μ_{cv} , we find

$$\mu_{11} = \left(\frac{2\xi}{1 + \xi^2} \right)^{3/2}, \quad \mu_{22} = \left(\frac{2\xi}{1 + \xi^2} \right)^{5/2}. \quad (\text{D3})$$

With $\xi = 1.23$, we get $\mu_{11} = 0.97$ and $\mu_{22} = 0.95$. Such values very close to unity are typical for strong confinement in a quantum dot. The energetic distance between both transitions equals $\Delta^c + \Delta^v = 115$ meV (without polaron corrections).

Apart from the parameter set deduced from the experimentally given level distances, we chose another one which has perfect resonance between the hole level distance and the LO phonon energy, i.e. $\Delta^v = 24$ meV. This yields a somewhat larger QD with $X_v = 2.66$ nm and $X_c = \xi X_v = 3.27$ nm, while keeping all the other parameters the same. The level distance for the electrons amounts to be $\Delta^c = 55$ meV, giving an energetic distance between the optically allowed transitions of 79 meV. We call this the *resonant* QD, while the parameter set backed by experiment is referred to as the *non-resonant* QD.

-
- [1] L. Bányai and S. W. Koch, *Semiconductor Quantum Dots* (World Scientific, Singapore, 1993).
 - [2] M. G. Bawendi, P. J. Carroll, W. L. Wilson, and L. E. Brus, *J. Chem. Phys.* **96**, 946 (1992).
 - [3] J.R. Guest, T.H. Stievater, D.G. Steel, D. Gammon, C. Ell, and H.M. Gibbs, *Phys. Rev. B* **65**, 241310 (2002).
 - [4] T. Flissikowski, A. Hundt, M. Lowisch, M. Rabe, and F. Henneberger, *Phys. Rev. Lett.* **86**, 3172 (2001).
 - [5] B. Bockelmann and G. Bastard, *Phys. Rev. B* **42**, 8947 (1990).
 - [6] O. Verzelen, R. Ferreira, and G. Bastard, *Phys. Rev. Lett.* **88**, 146803 (2002).
 - [7] S. Schmitt-Rink, D. A. B. Miller, and D. S. Chemla, *Phys. Rev. B* **35**, 8113 (1987).
 - [8] L. Besombes and K. Kheng and L. Marsal and H. Mariette, *Phys. Rev. B* **63**, 155307 (2001).
 - [9] A. Vagov and V.M. Axt and T. Kuhn, *Phys. Rev. B* **66**, 165312 (2002).
 - [10] E.A. Muljarov and R. Zimmermann, *Phys. Rev. Lett.* **93**, 237401 (2004).
 - [11] T. Stauber and R. Zimmermann and H. Castella, *Phys. Rev. B* **62**, 7336 (2000).
 - [12] K. Král and Z. Khás, *Phys. Rev. B* **57**, R2061 (1998).
 - [13] V. López-Richard and S. S. Oliveira and G.-Q. Hai, *Phys. Rev. B* **71**, 075329 (2005).
 - [14] M. I. Vasilevskiy and E. V. Anda and S. S. Makler, *Phys. Rev. B* **70**, 035318 (2004).
 - [15] R. Zimmermann and E. Runge, in *Proc. 26th ICPS, Edinburgh* (Inst. of Physics Publ., 2002).
 - [16] Y. Gu and Igor L. Kuskovsky and J. Fung and G. F. Neumark and X. Zhou and S. P. Guo and M.C. Tamargo, *phys. stat. sol. (c)* **1**, 779 (2004).
 - [17] M. Reed and B. Simon, *Methods of Modern Mathematical Physics I* (Academic Press, New York, 1975).
 - [18] I.A. Akimov and T. Flissikowski and A. Hundt and F. Henneberger, *phys. stat. sol. (a)* **201**, 412 (2004).
 - [19] G.D. Mahan, *Many-Particle Physics* (Plenum Press, New York, 1990).
 - [20] J. Puls and M. Rabe and H.-J. Wünsche and F. Henneberger, *Phys. Rev. B* **60**, R16303 (1999).
 - [21] O. Madelung, ed., *Semiconductors* (Springer, Berlin, 1986), Landolt-Boernstein New Series.